



Updated climatological mean $\Delta f\text{CO}_2$ and net sea–air CO_2 flux over the global open ocean regions

Amanda R. Fay¹, David R. Munro^{2,3}, Galen A. McKinley¹, Denis Pierrot⁴, Stewart C. Sutherland¹,
Colm Sweeney³, and Rik Wanninkhof⁴

¹Columbia University and Lamont-Doherty Earth Observatory, Palisades, NY, USA

²Cooperative Institute for Research in Environmental Sciences (CIRES),
University of Colorado, Boulder, CO, USA

³Global Monitoring Laboratory, National Oceanic and Atmospheric Administration, Boulder, CO, USA

⁴Atlantic Oceanographic and Meteorological Laboratory, National Oceanic and Atmospheric Administration,
4301 Rickenbacker Causeway, Miami, FL, USA

Correspondence: Amanda R. Fay (afay@ldeo.columbia.edu)

Received: 19 October 2023 – Discussion started: 24 October 2023

Revised: 14 March 2024 – Accepted: 20 March 2024 – Published: 2 May 2024

Abstract. The late Taro Takahashi (Lamont-Doherty Earth Observatory (LDEO), Columbia University) and colleagues provided the first near-global monthly air–sea CO_2 flux climatology in Takahashi et al. (1997), based on available surface water partial pressure of CO_2 measurements. This product has been a benchmark for uptake of CO_2 in the ocean. Several versions have been provided since, with improvements in procedures and large increases in observations, culminating in the authoritative assessment in Takahashi et al. (2009a, b). Here we provide and document the last iteration using a greatly increased dataset (SOCATv2022) and determining fluxes using air–sea partial pressure differences as a climatological reference for the period 1980–2021 (Fay et al., 2023, <https://doi.org/10.25921/295g-sn13>). The resulting net flux for the open ocean region is estimated as $-1.79 \pm 0.7 \text{ Pg C yr}^{-1}$, which compares well with other global mean flux estimates. While global flux results are consistent, differences in regional means and seasonal amplitudes are discussed. Consistent with other studies, we find the largest differences in the data-sparse southeast Pacific and Southern Ocean.

Key points.

- An updated surface water CO_2 climatology for 1980–2021 is created using the SOCAT database, following procedures of Takahashi et al. (2009a, b).
- A net air–sea CO_2 flux of $-1.79 \pm 0.7 \text{ Pg C yr}^{-1}$ is determined for near-global ocean coverage.

1 Introduction

As of the start of the 2020s, atmospheric carbon dioxide (CO_2) levels exceed 415 ppm on an annual basis, and the continued growth of the atmospheric reservoir represents a major societal concern due to the impact on the radiative balance of the atmosphere. Warming and associated environmental changes including sea level rise and ocean acid-

ification have adverse effects on countless aspects of terrestrial and marine ecosystems, which in turn impact the air–sea exchange of CO_2 and the trajectory of the atmospheric CO_2 levels. The annual assessment by the Global Carbon Project (Friedlingstein et al., 2022) estimated that net global ocean carbon uptake was nearly 3.0 Pg C per year, which corresponds to about a quarter of the total annual emissions (the total anthropogenic CO_2 emission, including the cement carbonation sink, was estimated at $10.9 \pm 0.8 \text{ Pg C yr}^{-1}$) (Friedlingstein et al., 2022). Given the importance of the ocean as a CO_2 sink, it is essential to continuously monitor changes and improve our understanding of the ocean's role in the global carbon cycle.

Over the last several decades, multiple approaches based on atmospheric and oceanic observations have been devel-

oped to measure the impact of the ocean on the global CO_2 cycle. These approaches include atmospheric inversions (Feng et al., 2019), global atmospheric O_2/N_2 (Manning and Keeling, 2006), ^{13}C measurements (Quay et al., 1992; Tans et al., 1993), ocean inventory approaches (Gruber et al., 2023), and the measurement of surface ocean and atmospheric CO_2 (Takahashi et al., 1993). All methods work towards the goal of elucidating the net flux of CO_2 from the atmosphere into the ocean. These different approaches have multiple advantages and disadvantages, depending on the time and spatial scale of interest. Directly measuring surface ocean and atmospheric CO_2 levels has the advantage, given sufficient measurements, of deriving spatial and temporal variability over the ocean surface on short temporal and spatial scales. This method provides valuable insights into key processes driving the uptake and emissions of carbon when combined with our understanding of ocean physics and biological activity.

The surface ocean and atmospheric CO_2 approach leverages available observations and the dynamic sea–air gradient between the partial pressure of carbon dioxide ($p\text{CO}_2$) in the surface ocean ($p\text{CO}_2^{\text{oc}}$) and the overlying atmosphere ($p\text{CO}_2^{\text{atm}}$), known as the delta $p\text{CO}_2$ ($\Delta p\text{CO}_2$) and typically defined as $p\text{CO}_2^{\text{oc}} - p\text{CO}_2^{\text{atm}}$. This difference is the thermodynamic driving force for the transfer of CO_2 into (negative) and out of (positive) the ocean. On average, the $\Delta p\text{CO}_2$ across the global oceans is becoming increasingly negative as atmospheric CO_2 levels steadily rise, leading to an increasing carbon sink. Limited regions around the globe are sources of CO_2 to the atmosphere, including the equatorial Pacific Ocean and other areas of persistent upwelling.

The late Taro Takahashi was a leader in efforts to characterize the air–sea CO_2 flux through the design and deployment of $p\text{CO}_2$ systems throughout the global oceans, and perhaps most importantly, Takahashi was a leader in efforts to assemble, evaluate, and construct global ocean climatologies from available $p\text{CO}_2^{\text{oc}}$ datasets. Building on early collaborative work looking at ocean sources and sinks of carbon (Tans et al., 1990), many versions of the ocean $p\text{CO}_2$ climatology have been presented in the literature (Takahashi et al., 1997, 2002, 2009a, 2014), henceforth referred to as T-1997, T-2002, T-2009a, and T-2014. The climatologies have been highly utilized and cited by carbon cycle researchers from around the world and form a basis for current advancements in quantifying the ocean carbon sink.

Here, we present an updated near-global climatological mean distribution and net sea–air CO_2 flux which represent the mean of ocean conditions over the last 4 decades. This climatology is unique compared to other advanced machine learning approaches (e.g., Rödenbeck et al., 2015) in that it interpolates in time and space using only the available $p\text{CO}_2$ data rather than using proxy variables for gap filling. This difference in methodology provides a valuable alternative approach to the ongoing effort to characterize the global ocean carbon sink. This benchmark is critical for global carbon as-

sessments, notably the Regional Carbon Cycle Assessment and Processes (RECCAP2; DeVries et al., 2023) effort.

Building on previous work by Takahashi and colleagues, we employ the same time–space interpolation method used in the previous versions of the Takahashi climatology (e.g., T-2002, T-2009a, and T-2014) to create the climatology. However, here we use the Surface Ocean CO_2 Atlas (SOCAT) v2022 database (Bakker et al., 2016, 2022) rather than the LDEO database curated by Taro Takahashi. We use the SOCAT database for this update because it is the most comprehensive database of available observations from international research groups. We have included the climatology produced using the most recent LDEO database (LDEOv2019; Takahashi et al., 2021) with data extending to 2019 in the figures and text in the Supplement, but our main findings will focus on the results from the SOCAT database.

2 Data

2.1 SOCAT database

The SOCAT database was first released in 2011 (Pfeil et al., 2013) and is updated annually (Bakker et al., 2016). Observations are reported as values of fugacity of CO_2 ($f\text{CO}_2$) in micro-atmospheres (μatm), along with a collection of ancillary data including concurrent observations such as sea surface temperature (SST) (more accurately the ship intake temperature), temperature of equilibration, salinity, and sea level pressure at the time of equilibration. The SOCAT database also includes supplemental variables with values interpolated from gridded global datasets such as satellite SST and National Centers for Environmental Prediction (NCEP) sea level pressure. The database restricts the included data to only observations that are measured in near-continuous operation or in discrete samples with an equilibrator system. This means that it does not include $f\text{CO}_2$ values that are calculated from other ocean carbon measurements including dissolved inorganic carbon, total alkalinity, and/or pH. For this analysis, we select SOCAT data from cruises with flags A–D and observations with a World Ocean Circulation Experiment (WOCE) flag of 2 (Pfeil et al., 2013). More information on the SOCAT database is available in Bakker et al. (2016); current and previous releases are available to download at <https://www.socat.info/index.php/data-access/> (last access: 18 September 2023).

The SOCAT database (Bakker et al., 2016) is the largest and most widely used collection of quality-controlled $f\text{CO}_2$ data with over twice the number of observations included in the latest LDEO database (LDEOv2019). In this work, we utilize the SOCATv2022 release which includes over 33.7 million observations spanning the years 1957 through to 2021 (<https://doi.org/10.25921/1h9f-nb73>, last access: 15 July 2022, Bakker et al., 2022). We use observations beginning in 1980 due to limited metadata available for earlier observations. This time restriction eliminates only 24 786 ob-

servations or less than 0.1 % of the total number of observations included in the SOCATv2022 release. We also exclude coastal observations collected within 100 km of land similar to past LDEO climatologies, which reduces the total number of observations utilized to just over 21.3 million. Unlike past LDEO climatologies, this climatology does not exclude observations collected in the equatorial Pacific during El Niño periods.

2.2 $f\text{CO}_2$ vs. $p\text{CO}_2$

For this climatology, we report values of the fugacity of carbon dioxide ($f\text{CO}_2$) rather than $p\text{CO}_2$. The $f\text{CO}_2$ is equal to the $p\text{CO}_2$ corrected for non-ideality of CO_2 solubility in water using the virial equation of state (Weiss, 1974). The fugacity correction for surface water is 0.996 and 0.997 at 0 and 30 °C, respectively (Dickson et al., 2007), or 0.7 to 1.2 μatm lower than the corresponding $p\text{CO}_2$, and it depends primarily on temperature for the conversion, although pressure is also included in the conversion equation. It is now common practice in the observational community to present observed values as $f\text{CO}_2$, and this option has been endorsed by the IOCCP (International Ocean Carbon Coordination Project). The correction of $p\text{CO}_2^{\text{occe}}$ and corresponding $p\text{CO}_2^{\text{atm}}$ values to $f\text{CO}_2$ is practically identical such that the resulting $\Delta f\text{CO}_2$ is always within 0.1 μatm compared to the corresponding $\Delta p\text{CO}_2$. As a result, this difference will not have a meaningful impact on air–sea flux calculations. Only at elevated $f\text{CO}_2$ levels, such as those in the subsurface ocean, is the difference between $f\text{CO}_2$ and $p\text{CO}_2$ significant. Therefore, the shift in this climatology from $p\text{CO}_2$ to $f\text{CO}_2$ simply aligns this updated climatology with current community best practices. This choice avoids conversions given that the SOCAT database reports $f\text{CO}_2$ values.

2.3 Distribution of measurements

At present, the SOCAT database relies on voluntary submission of quality-controlled data from over 100 scientists. The number of observations has increased significantly over the past decades, facilitated by a now-automated data submission process. Even with this increase in observations, there are only a few regions over the global oceans where $f\text{CO}_2^{\text{occe}}$ has been systematically monitored over multiple decades at nearly the same location (Bakker et al., 2016; Bates et al., 2014; Landschützer et al., 2016, Fig. 1). Of the observations considered in this analysis, spanning years 1980–2021, only 1.4 % of the monthly 1° by 1° global ocean grid cells have measured values. Most of the data (65 %) were collected since 2010.

An additional challenge to global monitoring efforts is that observations are not collected consistently throughout the annual cycle in many locations around the globe, thus requiring considerable interpolation to produce a full seasonal climatology. Much of the ocean contains data collected in

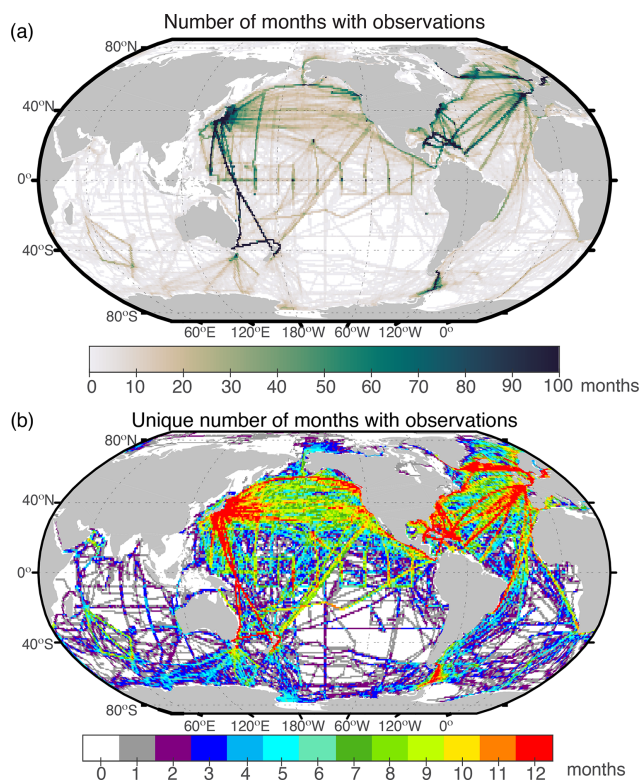


Figure 1. (a) Total number of months with at least one observation in each 1° grid cell in the SOCATv2022 database for years 1980–2021 (Bakker et al., 2022). The maximum number possible for a grid cell is 504 (42 years × 12 months). (b) The number of unique calendar months in each grid cell where at least one observation has been made since 1980. Red indicates grid cells where each month (January–December) has been sampled at least once over the (more than) 40-year time series, while white indicates grid cells with no measurements over the length of the time series.

fewer than three unique months of the year, regardless of how many years of data are available (Fig. 1b). Current efforts utilize proxy variables and machine learning to identify relationships between ocean carbon and better-observed variables (often SST, chlorophyll, mixed layer depth, etc.) and then through those relationships extrapolate available ocean $f\text{CO}_2$ to fill the missing months of the seasonal cycle. Unlike those methods (e.g., methods compared by Rödenbeck et al., 2015), we do not utilize any proxy variables in this method and only rely on available $f\text{CO}_2^{\text{occe}}$ values in the SOCAT database to estimate the seasonal climatology. Hence, this effort provides a complementary alternative interpolation method to other approaches.

2.4 Atmospheric $f\text{CO}_2$

For the calculation of atmospheric carbon dioxide, we utilize zonally invariant NOAA marine boundary layer (MBL) $x\text{CO}_2$ values which are reported in units of ppm or $\mu\text{mol mol}^{-1}$ (Lan et al., 2023) and provided with each

observation in the SOCAT dataset. In order to calculate $f\text{CO}_2^{\text{atm}}$ values from MBL $x\text{CO}_2^{\text{atm}}$ values, we follow standard operating procedures and equations outlined in Dickson et al. (2007) and use the SST, salinity, and sea level pressure observations also reported for each value in the SOCAT database (Bakker et al., 2022). The SST (more specifically ship intake temperature) is measured concurrently with surface ocean CO_2 , sea level pressure is from NCEP, and surface salinity is from the World Ocean Atlas (WOA). $\Delta f\text{CO}_2$ ($\Delta f\text{CO}_2$) is calculated by subtracting corresponding atmospheric values from ocean values ($f\text{CO}_2^{\text{oce}} - f\text{CO}_2^{\text{atm}}$).

3 Methods

3.1 Normalization to a reference year

In previous versions of the LDEO climatology, emphasis was placed on the calculation of trends in surface ocean carbon levels for all regions of the global ocean. These trends were used to normalize all available observations to one reference year by correcting for the estimated change that would be expected between the collection date of the observation and the reference year. In this updated climatology, we use $\Delta f\text{CO}_2$ values as input to the algorithm rather than allowing for the adjustment of $f\text{CO}_2^{\text{oce}}$ to a specific reference year. A similar methodology was used in early versions of the LDEO climatology (i.e., T-1997).

By utilizing this method to collapse all available data to 1 year, we make the assumption (as made by T-1997) that the ocean and atmosphere are changing at the same rate and thus that the $\Delta f\text{CO}_2$ has been constant over the (more than) 40 years of observations. This assumption allows for a standard method for the normalization of all observations to 1 calendar year. This method is utilized in contrast to the most recent LDEO climatologies where trends over distinct time periods were investigated and where one trend was then selected for use in time-normalization throughout much of the global ocean (i.e., T-2002, T-2009a, and T-2014).

Atmospheric $p\text{CO}_2$ change drives rising ocean $p\text{CO}_2$, and surface ocean carbon concentrations follow atmospheric increases on multidecadal timescales and over large regions and on the global scale (Fay and McKinley, 2013; McKinley et al., 2020). Large synthesis efforts by those in the global ocean carbon community show that even if ocean trends are larger/smaller than the atmosphere on decadal or multi-year time periods, when considering the longest time periods, the atmosphere and ocean carbon trends are statistically indistinguishable over much of the global ocean (Fay and McKinley, 2013; Tjiputra et al., 2014). While the Tjiputra et al. (2014) and Fay and McKinley (2013) efforts consider large regional analyses, Bates et al. (2014) provide a synthesis of trends in $p\text{CO}_2$ at long-term observing stations, with most of the stations showing a match to the rise in atmospheric CO_2 concentration (Tanhua et al., 2015).

Table S1 in the Supplement shows biome-scale mean $f\text{CO}_2$ trends computed using all available $1^\circ \times 1^\circ$ grid cells with observations in the gridded product released as part of SOCATv2022 (Sabine et al., 2013). We present seasonal trends for each biome due to seasonal sampling bias over much of the global oceans. Similar to T-2009a (see Tables 1–5 of T-2009a), trends for different ocean regions vary significantly (Table S1) due in part to differing years with available data across ocean regions (Fig. S5 in the Supplement). Observations within the Indian Ocean, for example, and other regions with blue shading in Fig. S5 are weighted towards the 1980s and 1990s, while regions stretching across the North Atlantic and North Pacific have been heavily sampled over the last 2 decades with ships of opportunity. These well sampled regions have median years of collected observations later than 2010 (areas with red shading in Fig. S5).

Recent studies (Friedlingstein et al., 2022) demonstrate that, globally, the oceans lag slightly behind the atmosphere in terms of rates of carbon increase; thus, $\Delta f\text{CO}_2$ has become increasingly negative as noted above. The central climatological year represented by our method is thus somewhat ambiguous regionally, though globally it is centered at about 2010. The median year of all $f\text{CO}_2$ observations collected in SOCATv2022 greater than 100 km from land is 2013. Since observations are more densely clustered in the recent period, observations in the early period may have a greater weight in determining climatological values. Given global trends, our approach may estimate a smaller ocean sink in regions where the ocean was sampled more heavily early in the time period (e.g., blue shading in Fig. S5) and a greater ocean sink in regions with heavy recent sampling (red shading in Fig. S5). We acknowledge that the assumption of a constant $\Delta f\text{CO}_2$ does not take into account the long-term trend in $\Delta f\text{CO}_2$; however, our simplified approach avoids application of trends determined for well-observed regions and time periods across poorly observed regions and time periods.

We conducted a sensitivity analysis to demonstrate the impact of the $\Delta f\text{CO}_2$ method implemented in this version versus a normalization approach similar to that applied in T-2009a. Specifically, we assumed a homogeneous $1.5 \mu\text{atm yr}^{-1}$ trend in $f\text{CO}_2^{\text{oce}}$ for all regions and years and normalized available observations to a reference year of 2010. Spatial maps of the differences in $f\text{CO}_2$ for the year 2010 for the normalization approach versus $\Delta f\text{CO}_2$ method are shown in the Supplement (Fig. S6). Globally, the annual ocean uptake created using the $1.5 \mu\text{atm yr}^{-1}$ normalization method (T-2009a) is within 3 % of the $\Delta f\text{CO}_2$ method (this analysis); specifically, the values are $-1.85 \text{ Pg C yr}^{-1}$ versus $-1.79 \text{ Pg C yr}^{-1}$ for the $1.5 \mu\text{atm yr}^{-1}$ normalization method and the presented $\Delta f\text{CO}_2$ approach, respectively, for a reference year of 2010.

3.2 Method for time–space interpolation

The method for spatial interpolation and day of year utilized in the climatology has not changed from the previous versions (e.g., T-2009a). As described above, $\Delta f\text{CO}_2$ values are used to compile observations into one reference year in contrast to the time-normalization approach of T-2009a. The spatial interpolation scheme requires that all observations are binned into $4^\circ \times 5^\circ$ grids for each day of the year. In some areas of the global ocean, such as the northern and equatorial ocean regions, there are observations in a majority of the pixels. However, vast expanses in the Southern Hemisphere have few observations in each pixel and there are many pixels that contain no observations at all (Fig. 1).

We follow the same methodology as T-2009a for binning observations in sparsely sampled grid cells south of 12°S . Here, spatial binning is increased by 4° and 5° longitude and latitude, respectively, extending from the center of each grid cell. This creates a grid of overlapping $8^\circ \times 10^\circ$ grid cells. Additionally, bins include the day before and after a given day of year. The mean is computed by weighting measured values inversely proportional to their time–space distance from the pixel center. After the above procedures are applied, more than 50 % of the space–time pixels over the global oceans are filled.

To estimate the $\Delta f\text{CO}_2$ values in the remaining cells, an interpolation equation based on the 2-D diffusion–advection transport of surface waters is used, as in T-2009a. The equation is discretized onto a $4^\circ \times 5^\circ$ grid for the global ocean, and it is solved iteratively using a finite difference algorithm (Takahashi et al., 1995; T-1997). The method avoids singularities at the poles by assigning land to each high-latitude region (Antarctica in the south and treating the highest latitudes of the Arctic Ocean as land in the north). With this method, the resulting $\Delta f\text{CO}_2$ values are the solutions obtained after 500 iterations, as previously determined on the basis of interpolation experiments of temperature values (T-2009a).

With this interpolation scheme, observed $\Delta f\text{CO}_2$ values where available are preserved, and the continuity equation is used to compute values for grid cells that have no observations. Consistent with previous iterations of this approach, the combined effects of internal sources and sinks of carbon, CO_2 exchange with the atmosphere, and upwelling of deep waters are all assumed to be included in the analysis of the observations that feed into the interpolation scheme. Uncertainties persist due to the sparsity of input data, normalization to a reference year, and the space–time interpolation. In part to address these uncertainties, we report only monthly means.

To maintain consistency with similar products and input datasets for flux calculations, we downscale to 1° boxes by assigning all twenty $1^\circ \times 1^\circ$ pixels in a $4^\circ \times 5^\circ$ grid cell the same $\Delta f\text{CO}_2$ value. When calculating sea–air fluxes, because the other inputs to the flux calculation such as wind

speed are varying on a $1^\circ \times 1^\circ$ resolution grid, differences in the gridded flux climatology emerge on this finer spatial scale.

3.3 Flux calculation method: pySeaFlux

To assess the near-global ocean carbon sink associated with these $\Delta f\text{CO}_2$ estimates, air–sea CO_2 exchange must be calculated. The gridded monthly $1^\circ \times 1^\circ$ $\Delta f\text{CO}_2$ values were used to compute air–sea CO_2 fluxes using the bulk formulation with Python package pySeaFlux v1.3.1 (<https://github.com/lukegre/SeaFlux>, last access: 1 June 2023; Gregor and Fay, 2021). The net sea–air CO_2 flux (F) is estimated using

$$\text{Flux} = kw \cdot \text{sol} \cdot (f\text{CO}_2^{\text{oce}} - f\text{CO}_2^{\text{atm}}) \cdot (1 - \text{ice}) \quad (1)$$

where kw is the gas transfer velocity, sol is the solubility of CO_2 in seawater (in units of $\text{mol m}^{-3} \mu\text{atm}^{-1}$), $f\text{CO}_2^{\text{oce}}$ is the partial pressure of carbon in the surface ocean (in μatm), and $f\text{CO}_2^{\text{atm}}$ (in units of μatm) represents the atmospheric CO_2 levels in the marine boundary layer. Finally, to account for the seasonal ice cover at high latitudes, the fluxes are weighted by one minus the ice fraction (ice), i.e., the open ocean fraction. By utilizing the pySeaFlux package (Fay et al., 2021; Gregor and Fay, 2021), we are able to include multiple scaled gas transfer velocities for three different wind products, and our resulting flux estimate is a mean of the three. Additional inputs to the flux calculation include EN4.2.2 salinity (Good et al., 2013), SST and ice fraction from NOAA Optimum Interpolation Sea Surface Temperature V2 (OISSTv2; Reynolds et al., 2002), and European Centre for Medium-Range Weather Forecasts (ECMWF) ERA5 sea level pressure (Hersbach et al., 2023). Finally, surface winds and the associated wind scaling factor for the Cross-Calibrated Multi-Platform v2 (CCMP2; Atlas et al., 2011), the Japanese 55-year Reanalysis (JRA-55; Kobayashi et al., 2015), and the ECMWF ERA5 (Hersbach et al., 2023) reanalysis products are used.

Fluxes reported here use inputs from the year 2010 for the kw , sol , and ice fraction variables. Alternatively, we have calculated fluxes using a mean over a 17-year time period centered on the year 2010. This yields a very similar value with the mean difference being a $0.04 \text{ Pg C yr}^{-1}$ increase in estimated carbon uptake.

4 Results

4.1 Climatological mean distribution of surface water $\Delta f\text{CO}_2$

4.1.1 Global

The near-global 12-month climatological mean distribution of $\Delta f\text{CO}_2$ ($f\text{CO}_2^{\text{oce}}$ minus $f\text{CO}_2^{\text{air}}$) is reported for the SOCAT database (Fig. 2; Fay et al., 2023). Evident in the mapped climatology are the large-scale patterns across the

global ocean: the consistent high (positive) $\Delta f\text{CO}_2$ values in the equatorial Pacific region where upwelling is a dominant influence and low (negative) values of $\Delta f\text{CO}_2$ in the North Atlantic region where evaporation leads to increased salinity and cooling, driving strong uptake of carbon and subduction of surface waters.

A near-global mean climatology curve shows a bimodal shape in $\Delta f\text{CO}_2$, with a smaller peak in boreal spring (March/April) and a much larger peak in late boreal summer (August/September), clearly driven by the hemispheric seasonal cycles (Fig. 2a). The global curve reaches its minimum in November and begins a recovery throughout the boreal winter before dipping again to a springtime minimum in June. The near-global annual mean $\Delta f\text{CO}_2$ value is $-4.1 \mu\text{atm}$ (with temporal standard deviation equal to $1.6 \mu\text{atm}$), and it is notable that the global mean $\Delta f\text{CO}_2$ value is below zero for every month of the year, suggesting that seasonally the global ocean mean is a perpetual carbon sink with expansive regions of uptake nearly always outweighing smaller regions of efflux (Figs. 2, 3). On the other hand, the northern and southern hemispheric seasonal cycles each exhibit peaks in $\Delta f\text{CO}_2$ above zero during their corresponding warm/summer months (Fig. 2a).

4.1.2 Regional

To show the seasonal changes in $\Delta f\text{CO}_2$ more clearly, it is valuable to consider the patterns exhibited over consistent biogeochemical regions around the globe. For this analysis, we utilize the biomes of Fay and McKinley (2014), but for simplicity we combine the seasonally stratified and permanently stratified subtropical biomes into one region in the Northern Hemisphere (referred to simply as subtropical in this article). Monthly climatologies for each of the biomes are shown (Fig. 4) in addition to the grid-scale maps for each climatological month which allows for further regional interpretation (Fig. 3). Table 1 lists the annual mean $\Delta f\text{CO}_2$ values in each of these regions.

The equatorial regions of the Pacific and Atlantic oceans have positive $\Delta f\text{CO}_2$ values throughout the annual cycle and little seasonal variability. This indicates that the area is a source of CO_2 to the atmosphere year round. The equatorial Pacific (Fig. 4b) has the highest positive $\Delta f\text{CO}_2$ values (annual mean = $35.4 \mu\text{atm}$), followed by the tropical Atlantic (Fig. 4a; annual mean = $14.8 \mu\text{atm}$).

The subtropical biomes, representing the temperate North and South Atlantic and Pacific basins exhibit large seasonal $\Delta f\text{CO}_2$ cycles which change sign throughout the year. Here, the $\Delta f\text{CO}_2$ cycle is largely temperature driven. Positive $\Delta f\text{CO}_2$ in warm summer months and negative values in colder winter months, reflecting the dominance of seasonal temperature changes on the cycles of ocean $f\text{CO}_2$ in these regions. The seasonal amplitude for the subtropical North Pacific is $44.7 \mu\text{atm}$, and it is slightly larger than the seasonal amplitude in the subtropical North Atlantic

($42.7 \mu\text{atm}$). Since the mean seasonal amplitudes for SST are quite similar in these two ocean basins, with the Atlantic having a slightly larger seasonal change in surface temperature (4.4°C in Pacific and 5.0°C in Atlantic; not shown), the difference in $\Delta f\text{CO}_2$ amplitudes between the Pacific and Atlantic subtropical regions cannot be attributed solely to SST, and it may reflect differences in biogeochemical cycling between these two basins.

Seasonal changes in the northern subtropical oceans are roughly 6 months out of phase from the southern subtropical biomes. The South Pacific subtropical biome has a seasonal amplitude of $29.8 \mu\text{atm}$ which is nearly $15 \mu\text{atm}$ smaller than that of the North Pacific subtropical biome. In contrast, the seasonal amplitude of the South Atlantic subtropical basin is just $1 \mu\text{atm}$ smaller than its counterpart in the North Atlantic (the South Atlantic subtropical amplitude is $41.7 \mu\text{atm}$). The Indian Ocean subtropical biome which encompasses most of the Indian Ocean, both above and below the Equator, has a smaller $\Delta f\text{CO}_2$ amplitude ($22.3 \mu\text{atm}$), but the phasing matches well with both the South Pacific and South Atlantic subtropical biomes, with peak (positive) $\Delta f\text{CO}_2$ values in February and the lowest values in August. The smaller $\Delta f\text{CO}_2$ seasonal amplitudes in the Indian and South Pacific subtropical basins are partially attributable to lower SST variability in these regions (SST seasonal cycle amplitudes are 4.0 and 3.0°C in the South Pacific and Indian subtropics, respectively, compared to 4.6°C in the subtropical South Atlantic). However, it is likely that both differences in spatiotemporal patterns of primary productivity and under-sampling in the South Pacific and Indian subtropics (Fig. 1) also contribute to differences in $\Delta f\text{CO}_2$ seasonal amplitudes between these basins.

The timing of the $\Delta f\text{CO}_2$ trough in the subpolar regions is opposite that of the subtropical North Pacific and Atlantic basins. Strongly negative $\Delta f\text{CO}_2$ in the spring and summer months is due to the effects of intense biological drawdown which quickly and dramatically lowers carbon levels in the subpolar surface ocean with the onset of the growing season. Biological productivity and strong spring/summer stratification result in subpolar seasonal cycles that are roughly 4 to 6 months out of phase compared to adjacent subtropical regions. In the Atlantic subpolar biome, $\Delta f\text{CO}_2$ values are consistently below zero throughout the annual cycle (a maximum of $-15.1 \mu\text{atm}$ occurs in February). In the subpolar North Pacific basin, positive $\Delta f\text{CO}_2$ values are present over the boreal winter (January–March) before biological drawdown associated with the spring bloom lowers the $\Delta f\text{CO}_2$ values back below zero for the remainder of the year. The spring drawdown is weaker in the subpolar North Pacific compared to the subpolar North Atlantic.

Figure 4c displays the seasonal cycle for the Southern Ocean biomes including the seasonal ice biome, the subpolar region, and the seasonally stratified subtropical region of the Southern Hemisphere. The higher latitude subtropical region has negative $\Delta f\text{CO}_2$ values throughout the year and

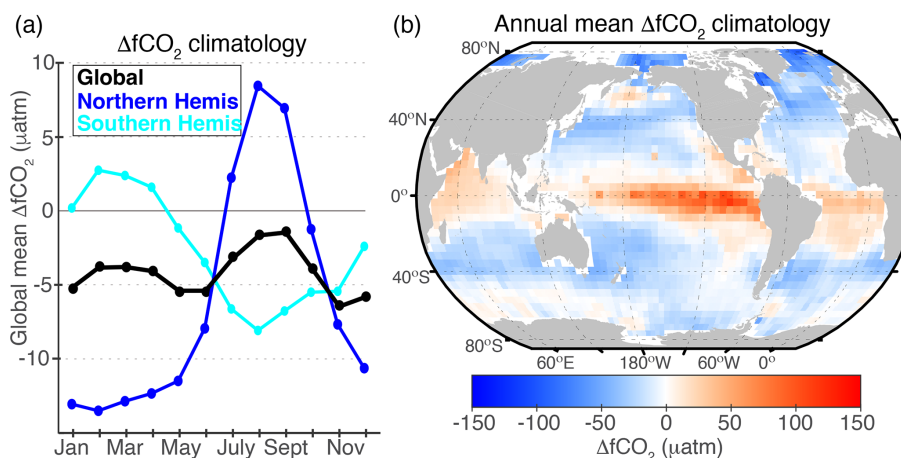


Figure 2. (a) Global mean and Northern Hemisphere and Southern Hemisphere $\Delta f\text{CO}_2$ seasonal climatology from the SOCAT database. (b) Map of annual $\Delta f\text{CO}_2$ climatology.

a relatively small seasonal $\Delta f\text{CO}_2$ amplitude compared to the more expansive South Atlantic, South Pacific and Indian subtropical basins to the north. The mean $\Delta f\text{CO}_2$ and seasonal amplitude for the Southern Ocean subtropical region is -22.5 and 9.0 μatm , respectively.

The Southern Ocean subpolar and ice biomes both have relatively strong seasonal cycles, reaching maximums of $\Delta f\text{CO}_2$ near and slightly above zero, respectively, during the late austral winter and early austral spring (Fig. 4c). This positive peak during July through October in the Southern Ocean seasonal ice zone is influenced by under-ice vertical mixing with deep waters that contain excess carbon and nutrients. During the austral spring and summer months, intense phytoplankton blooms occur near and around the edges of the retreating sea ice in the seasonal ice zone and within the subpolar region. These blooms cause dramatic drops in $\Delta f\text{CO}_2$ values at the end of the calendar year (October–December). Limited sampling and smoothing from the interpolation method fail to capture the high spatiotemporal variability that characterizes this highly dynamic region.

4.2 Net air–sea CO_2 flux

The mean climatological global air–sea CO_2 flux estimate using the SOCAT database is -1.79 Pg C yr^{-1} , indicating uptake of carbon by the ocean. This is a slightly greater flux into the ocean than the direct estimate from the previous version of the climatology (T-2009a), which reported a direct estimated global mean flux of -1.4 Pg C yr^{-1} for the year 2000. For the uncertainty in global ocean–atmosphere CO_2 flux, we use the methods described in T-2009a with updated uncertainty estimates as reported when applicable. Wanninkhof et al. (2013) followed the same approach as T-2009a with consideration of updated synthesis work (Ho et al., 2011). Our approach combines uncertainty contributions from the spatial (13 % or ± 0.23 Pg C yr^{-1} ; T-2009a) and

temporal (± 0.5 Pg C yr^{-1} ; T-2009a) sampling of $\Delta f\text{CO}_2$ as well as smaller contributions for the uncertainty in the gas exchange parameterization (20 % or ± 0.36 Pg C yr^{-1} ; Wanninkhof, 2014), wind (± 0.09 Pg C yr^{-1} ; Fay et al., 2021), and riverine carbon (± 0.2 Pg C yr^{-1} ; Jacobson et al., 2007). This yields an uncertainty estimate of ± 0.7 Pg C yr^{-1} (when summed in quadrature) on our mean climatological global air–sea CO_2 flux estimate.

Results discussing the net flux produced from the LDEO $p\text{CO}_2$ database climatology are included in the Supplement.

4.2.1 Mean annual distribution

The near-global mean flux estimate presented here represents 90 % of the surface area of the global ocean. Specifically, this estimate excludes the coastal ocean and areas of the high-latitude seas. We have chosen to present the near-global flux value discussed above without any adjustment which could account for missing areas. Suggested methods for filling missing ocean areas in such reconstructions are available in Fay et al. (2021) but are not implemented in this climatology to remain consistent with its previous versions. An estimate of the flux from regions missing from this product can be obtained by using the full-coverage $p\text{CO}_2$ climatology combining open and coastal oceans (Landschützer et al., 2020). Considering only grid cells in the Landschützer et al. (2020) product that are missing in this climatology, we estimate an annual average coastal and high-latitude flux of -0.38 Pg C yr^{-1} . The flux adjustment for missing areas of this climatology varies throughout the seasonal cycle, ranging from -0.43 to -0.31 Pg C yr^{-1} during the 12 months of the climatology. This quantity is not included in the climatological estimate presented here.

Figure 5 shows the climatological mean annual sea–air CO_2 flux ($\text{mol m}^{-2} \text{yr}^{-1}$) and maps of two seasons (DJF and JJA) are displayed in Fig. 6. Annual mean sea–air CO_2

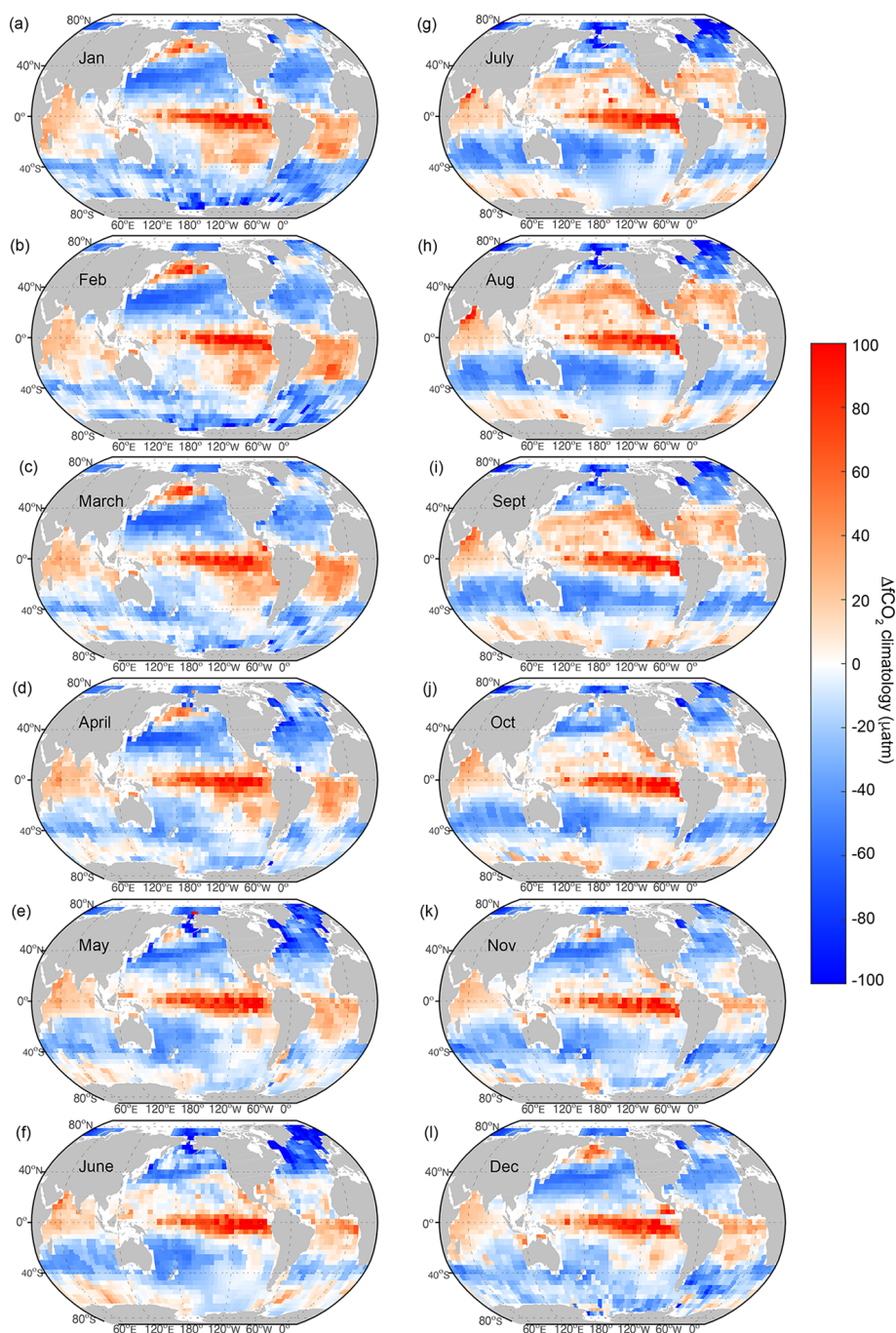


Figure 3. Monthly mean values for sea–air $\Delta f\text{CO}_2$. Warm colors indicate positive $\Delta f\text{CO}_2$ (ocean is greater than atmospheric CO_2), white indicates near zero $\Delta f\text{CO}_2$, and cool colors indicate negative $\Delta f\text{CO}_2$ (ocean CO_2 is lower than the atmosphere).

flux values for the ocean regions are summarized in Table 1. The equatorial Pacific is the most prominent atmospheric CO_2 source region, with a seasonally persistent sea-to-air flux of $0.35 \text{ Pg C yr}^{-1}$. When combined with the equatorial Atlantic region, the tropical belt emits an annual mean of $0.39 \text{ Pg C yr}^{-1}$ to the atmosphere. Adjacent to this tropical efflux zone are vast expanses of seasonally variable flux pat-

terns. The subtropical basins in both hemispheres act as CO_2 sinks in the cooler months and transition to regions of neutral or small CO_2 sources during the warmer months. At higher subtropical latitudes, strong winds and relatively low ocean $f\text{CO}_2$ values occur along the subtropical convergence zone where the cooled subtropical gyre waters with low $f\text{CO}_2$

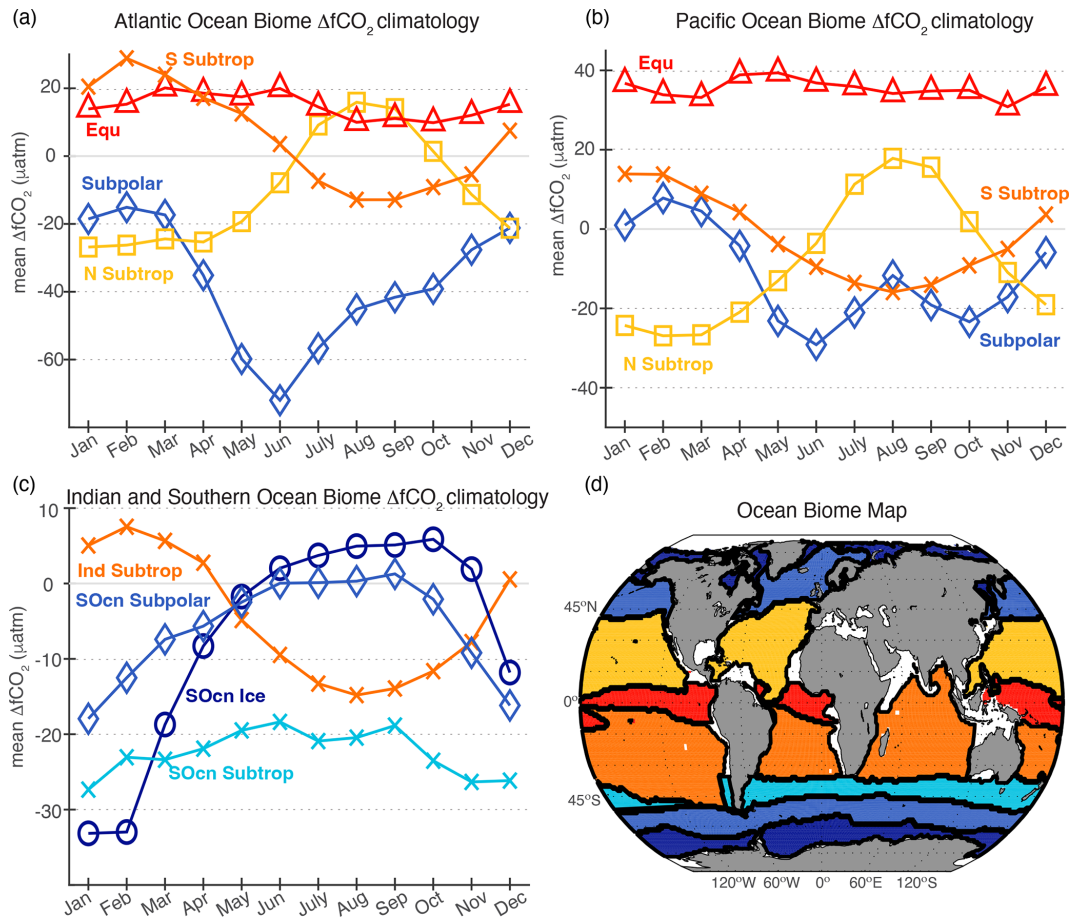


Figure 4. Monthly climatology of $\Delta f\text{CO}_2$ for each regional ocean biome in the (a) Atlantic, (b) Pacific, and (c) Indian and Southern Ocean basins. (d) Map of regional biomes. Colors of curves correspond to regions on the map in panel (d), with labels in matching colored text. Note that the y axis varies between subplots. Values for each region’s annual mean and standard deviations are listed in Table 1.

Table 1. Mean annual $f\text{CO}_2$ and flux in global open ocean biomes (Fay and McKinley, 2014). Value in parentheses is 1 standard deviation over the 12-month climatology. Area of each biome is also included. NP: North Pacific; SP: South Pacific; NA: North Atlantic; SA: South Atlantic; SO: Southern Ocean. SPSS: subtropical seasonally stratified; STSS: subtropical seasonally stratified. Northern Hemisphere subtropical regions are reported to match the regions shown in Fig. 4 (combining the permanently and seasonally stratified subtropical biomes from Fay and McKinley, 2014, into one).

Biome	$\Delta f\text{CO}_2$ (μatm)	Flux (Pg C yr^{-1})	Area (10^6 km^2)
NP ice	−24.6 (9)	−0.02 (0.02)	4.2
NP SPSS	−11.5 (12)	−0.11 (0.11)	12.8
NP subtropics	−8.2 (16)	−0.40 (0.53)	47.9
Pacific equ.	35 (2)	0.35 (0.03)	26.4
SP subtropics	−2.3 (10)	−0.14 (0.31)	52.7
NA ice	−19.3 (4)	−0.04 (0.01)	4.5
NA SPSS	−36.2 (17)	−0.27 (0.08)	9.7
NA subtropics	−10.0 (16)	−0.24 (0.26)	23.4
Atlantic equ.	14.7 (3)	0.04 (0.01)	7.4
SA subtropics	5.6 (14)	0.01 (0.12)	18.1
Indian subtropics	−4.5 (8)	−0.18 (0.16)	35.9
SO STSS	−22.1 (3)	−0.59 (0.06)	29.6
SO SPSS	−6.0 (6)	−0.21 (0.22)	30.7
SO ice	−6.8 (14)	−0.08 (0.12)	18.7

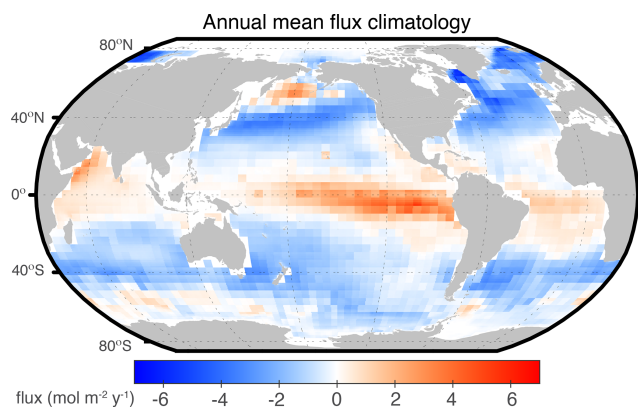


Figure 5. Annual mean CO_2 flux calculated from the SOCAT database. Flux is calculated using the SeaFlux method using the mean of three wind speed reanalysis products. Warm and cool colors indicate regions of carbon efflux and uptake, respectively. The near-global mean flux is $-1.79 \text{ Pg C yr}^{-1}$.

values meet the subpolar waters with biologically lowered $f\text{CO}_2$.

The Northern Hemisphere mid- and high-latitude regions represent a smaller sink compared to the corresponding regions of the Southern Hemisphere (Table 1), largely due to the overall greater surface area of the oceans in the Southern Hemisphere (oceans south of 35° S are 25 % of total global ocean area, while oceans north of 35° N are 15 % of total ocean area). The dramatic influence of the expansive Southern Hemisphere oceans is also demonstrated by the large flux in the Southern Ocean subtropical region ($-0.59 \text{ Pg C yr}^{-1}$) that represents 8 % of the global ocean surface area.

Moving poleward, a strong sink ($-0.27 \text{ Pg C yr}^{-1}$) occurs in the North Atlantic subpolar region which includes the Nordic Seas and the portions of the Arctic Ocean which contain observations. This strong localized carbon sink is attributed to the import of low anthropogenic waters at depth in the Gulf Stream that are exposed as mixed layers deepen (Ridge and McKinley, 2020) and to large phytoplankton blooms in spring followed by cooling in winter. In the Southern Ocean, annual mean CO_2 flux is heterogeneous and relatively small in the seasonal ice zone due to the ice cover that reduces sea–air gas transfer in winter. Additionally, the small annual flux values in the Southern Ocean subpolar and ice regions (-0.21 and $-0.08 \text{ Pg C yr}^{-1}$, respectively) are a result of a cancellation of the seasonal source (winter) and sink (summer) fluxes.

4.2.2 Seasonal variation of sea–air CO_2 flux

Seasonal variations in air–sea fluxes are clearly seen in the climatology (Fig. 6) and are attributed to a combination of effects including fluctuations in SSTs, biological uptake of carbon dioxide, and mixing and wind speeds.

The seasonal variability of fluxes in higher latitudes of the subtropics in the Atlantic, Indian, and Pacific oceans cause an oscillation from neutral or weak sources of CO_2 to the atmosphere in the warmer seasons to strong CO_2 sinks in the cooler or winter seasons. Water cools as it is transported poleward by western boundary currents, allowing for carbon uptake (Ayers and Lozier, 2012). In spring and summer, the biological drawdown of carbon increases CO_2 uptake by the ocean, partially offset by increases in $f\text{CO}_2$ due to warming.

Subtropical gyre regions also transition from weak sinks in the winter seasons to weak sources in the summer seasons, following the seasonal SST cycles and reflecting the dominance of temperature effects in controlling the seasonal variability in the $f\text{CO}_2$ and sea–air fluxes in oligotrophic gyres. In tropical low-latitude regions, seasonality is generally smaller; however, localized hot spots of high variability and large fluxes do exist, such as in the northwestern Indian Ocean where the strong summer monsoon winds force upwelling of carbon-rich subsurface waters and cause high gas transfer rates in this region (Chen and Tsunogai, 2019; T-2002; Sabine et al., 2000). The equatorial Pacific and Atlantic show little seasonal variability in CO_2 flux with a persistent efflux throughout the year.

In the Southern Ocean, there is a consistent region of moderate carbon source waters located in the Atlantic and Indian Ocean sector south of 45° S latitude during the austral winter (Fig. 6b). The source in the Southern Ocean region could be influenced by high $f\text{CO}_2$ waters from margins of the Antarctic sea-ice field given that the efflux values occur during the austral winter months (JJA). As the seasons transition to warmer temperatures and the ice edge recedes, this region is impacted by high rates of photosynthesis, causing $f\text{CO}_2$ drawdown and resulting in a transition to moderate carbon sinks during the austral summer (DJF). Another possibility is that the austral winter carbon source is linked to deep mixing and/or upwelling water which would bring an import of high dissolved inorganic carbon (DIC) to the surface layers. Given the limited number of observations, particularly in winter in the Southern Ocean (Fig. 1), confidence in the resulting climatology is lower in this region.

5 Discussion

It should be noted that there is not one specific reference year for this release of the $\Delta f\text{CO}_2$ climatology as was the case for previous releases (e.g., the year 2000 reference in T-2009a). Instead, this climatology represents a multidecadal time period, beginning in 1980, with the majority of observations feeding into the climatology collected after 2010. Therefore, while the $\Delta f\text{CO}_2$ climatology is not reported for a specific reference year, it is most representative of the conditions over the past 2 decades. We note, however, that the flux estimates given in this analysis are based on inputs from a single year, the year 2010, as described above in Sect. 3.3 (comparison

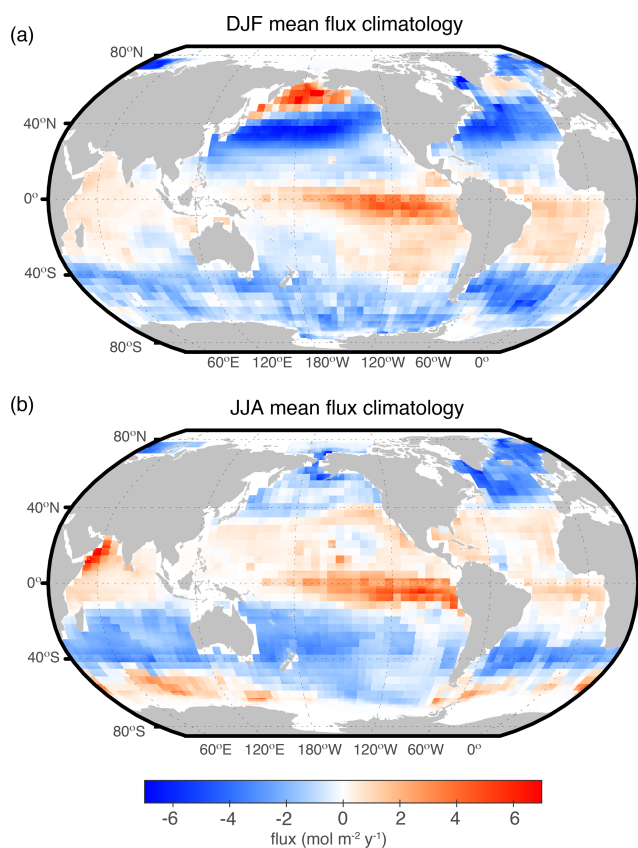


Figure 6. Seasonal sea–air CO_2 flux ($\text{mol C m}^{-2} \text{ yr}^{-1}$) climatology for (a) December–January–February (DJF) and (b) June–July–August (JJA). Positive values (warm colors) indicate sea-to-air fluxes (ocean efflux), and negative values (cool colors) indicate air-to-sea fluxes (ocean uptake).

of flux estimates using 2010 inputs and averages over several decades yield very similar results, also as described in Sect. 3.3).

5.1 Comparison with the T-2009a climatology

In the previous release of this climatology (T-2009a), $p\text{CO}_2$ values were corrected to a reference year of 2000 using a mean atmospheric CO_2 increase rate of $1.5 \mu\text{atm yr}^{-1}$ over the entire ocean area with the exception of the Bering Sea, where the observed rate of $-1.2 \mu\text{atm yr}^{-1}$ was used. In our updated method described above (Sect. 3.1), we eliminate the need to apply a normalization rate for observations and instead calculate a $\Delta f\text{CO}_2$ value for each observation using a colocated concurrent atmospheric $f\text{CO}_2$ value. We note that T-2014 presents a more updated $p\text{CO}_2$ climatology than T-2009a. Since T-2014 emphasizes climatologies for the other carbonate system variables (pH, dissolved inorganic carbon, and total alkalinity) and omits estimation of fluxes, we focus our comparison on values presented in T-2009a.

Spatial differences between the climatology created from surface water $\Delta f\text{CO}_2$ values using the methods discussed above and the approach of T-2009a (3 million observations) are shown in Fig. 7 for the months of February and August – months were selected for consistency with past comparisons presented in T-2009a and T-2002. The differences between this updated release and previous versions producing climatologies for reference years 2000 (T-2009a) and 1990 (T-1997) are unlikely to represent real change in the oceans over time, but they instead primarily reflect the impact of the greatly expanded database as well as the use of the $\Delta f\text{CO}_2$ approach as opposed to the time-normalization method of T-2009a (Fig. S9).

The most significant regional differences between this updated version and that of T-2009a are observed over the sub-polar North Atlantic, the subtropical Southeast Pacific, and portions of the Southern Ocean. In the North Atlantic, differences between versions are largest in the boreal winter (February map, top panel of Fig. 7) when the updated climatology exhibits less uptake compared to the T-2009a version (positive values on the map indicate more negative values in the T-2009a version). Differences in the North Atlantic can be at least partially attributed to the much greater availability of observations in this region between the two databases (Figs. 1, S1, S9). This is discussed in further detail in the Supplement text.

The Southeast Pacific is an area with very limited observations, but a few key datasets have been included in the SOCAT database since 2010. Figure 1 shows that despite these recent additions to SOCAT, there are still only a few observations covering this region. Comparison of Fig. 3 in this study with Fig. 9 of T-2009a suggests that the additional datasets in SOCATv2022 result in a more defined seasonal cycle for $f\text{CO}_2$ in the subtropical Southeast Pacific in the current release. Specifically, the map of differences shown in Fig. 7 shows that this region is a greater source of carbon to the atmosphere in austral summer and a greater sink in austral winter compared to T-2009a (compare also Fig. 6 of this study with Fig. 15 of T-2009a). In contrast, monthly maps included in Fig. 3 of T-2009a show little seasonal contrast in $\Delta p\text{CO}_2$ likely due to a lack of observations.

In the Southern Ocean region during austral winter (August), $\Delta f\text{CO}_2$ values are more negative in the current version compared to T-2009a. The Southern Ocean is also a region of limited data availability, particularly in austral winter, but one where SOCATv2022 also includes several datasets added in the past decade that have an outsized influence on the resulting climatology.

5.2 Comparison to other flux estimates

The estimate presented here for annual global mean carbon flux ($-1.79 \text{ Pg C yr}^{-1}$) represents slightly less uptake than reported by other studies, but given uncertainties, as well as differing time frames, spatial coverage, and gap-filling

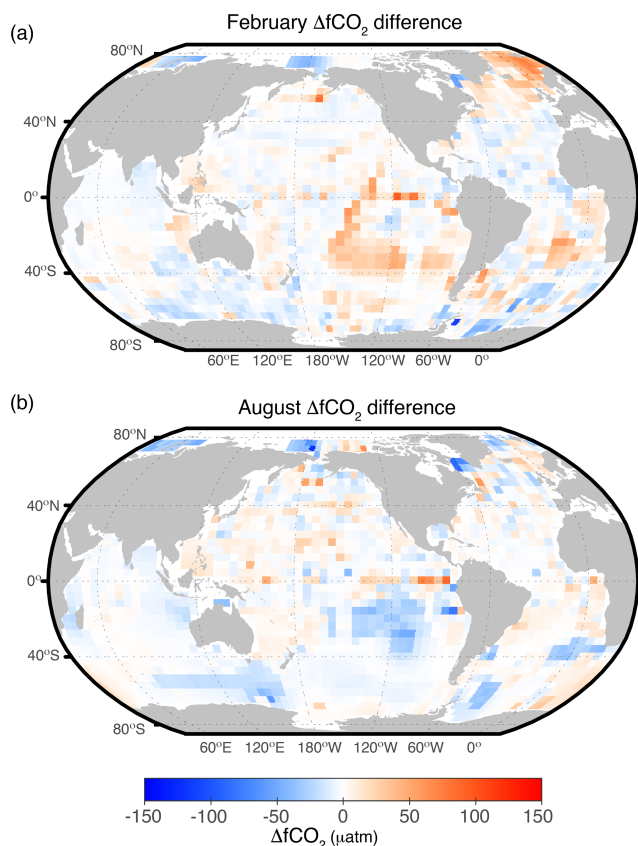


Figure 7. Difference maps for the surface water $\Delta f\text{CO}_2$ climatology produced by this study using SOCAT and that from T-2009a (maps show this study *minus* T-2009a) in (a) February and (b) August. In T-2009a, the ΔCO_2 values are reported as $p\text{CO}_2$, and here we are using $f\text{CO}_2$.

methodologies, our estimate compares closely with current estimates similarly based on observed surface ocean $f\text{CO}_2$.

To compare our new climatological estimate of contemporary air–sea net flux from surface ocean $f\text{CO}_2$ with estimates of the anthropogenic carbon flux from interior data (e.g., Gruber et al., 2019) or estimates from global ocean biogeochemical models (e.g., Friedlingstein et al., 2022; Hauck et al., 2020), it is necessary to account for the outgassing of natural carbon supplied to the ocean by rivers. This riverine estimate varies significantly in magnitude between studies and continues to be a research focus for the ocean carbon community. Therefore, we focus on comparisons between our climatological estimate and a mean carbon flux estimate from an ensemble of observation-based $p\text{CO}_2$ products included in the SeaFlux product (Fay et al., 2021).

The SeaFlux products span the years 1985–2020, are all similarly based on the SOCAT database, but employ various methods of machine learning and interpolation to produce full-coverage ocean carbon maps. For this comparison, a climatology of the SeaFlux product is produced, and fluxes are calculated in the same manner as for the

climatology presented here. Following this approach, the SeaFlux climatology ensemble yields a global mean flux of $-2.10 \text{ Pg C yr}^{-1}$, which represents a slightly larger flux into the ocean than that produced by the updated climatology ($-1.79 \pm 0.7 \text{ Pg C yr}^{-1}$). The differences in global flux can be attributed to the true global coverage of the SeaFlux product relative to the 90 % global ocean coverage of this study. As mentioned above in Sect. 4.2, an estimate of missing coastal and high-latitude fluxes increases the ocean carbon uptake estimate for this climatology by roughly $0.38 \text{ Pg C yr}^{-1}$. Adding this additional flux brings our analysis within 0.1 Pg C yr^{-1} of the SeaFlux ensemble (-2.17 versus $-2.10 \text{ Pg C yr}^{-1}$ for this analysis versus the SeaFlux estimate, respectively).

Spatially, comparison of the SeaFlux ensemble of products to our climatology shows strong agreement in overall patterns but significant differences in the mid- and high-latitude Southern Hemisphere oceans (Fig. 8). Gloege et al. (2021) analyzed a machine learning method’s ability to reconstruct global carbon fluxes from available observations using a test-bed approach and found the highest flux bias in the Southern Ocean regions as well as an overestimation of decadal variability in this region. Given the limited availability of year-round observations at high Southern Hemisphere latitudes, and the resulting reliance on various gap-filling approaches, it is not surprising that the largest differences between the climatology presented here and the SeaFlux ensemble emerges in this region. Significant differences between these climatologies are also evident in the high latitude North Pacific and North Atlantic, specifically in the boreal winter season (Fig. 8a). Again, a lack of observations in these regions during the winter season (Fig. 1) likely accounts for much of this disagreement, with more reliance on the interpolation methods used by each method. Machine learning methods that utilize proxy variables to estimate $p\text{CO}_2$ in unsampled areas, such as those in the SeaFlux product, often rely on relationships derived from better-observed areas that are deemed similar in biogeochemical characteristics and it is likely that the mechanisms at these high-latitude locations are not accurately captured by any available interpolation methods. This is also a current focus of research for the ocean-carbon-observing community.

6 Data availability

The updated climatology is available via the National Center for Environmental Information (NCEI) at <https://doi.org/10.25921/295g-sn13> (Fay et al., 2023).

7 Conclusion

An updated climatological mean distribution for $\Delta f\text{CO}_2$ (surface water minus atmosphere) using the methods of T-2009a is presented. This climatology is based on approxi-

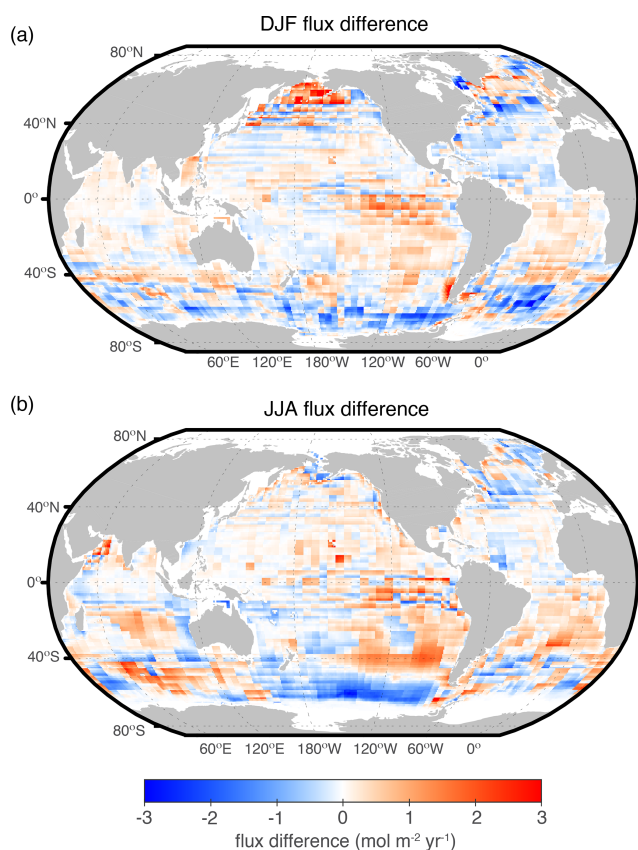


Figure 8. Difference map for carbon fluxes ($\text{mol m}^{-2} \text{yr}^{-1}$) calculated from this $\Delta f\text{CO}_2$ climatology and fluxes reported by an ensemble of observation-based products included in the SeaFlux product for (a) boreal winter, DJF, and (b) boreal summer, JJA. Map shows the difference defined as this study *minus* SeaFlux. Note that white areas at the poles are due to ice coverage extent (and therefore no value reported in the climatology) and not a flux difference of zero.

mately 7 times more open ocean observations from the SOCATv2022 database (over 21 million values, spanning years 1980–2021) compared to the 3 million data values used in T-2009a (and more than 3 times the approximately 6.5 million observations used in T-2014). In this updated climatology, observations made during El Niño periods over the equatorial Pacific are included, unlike climatologies presented by T-1997, T-2002, T-2009a, and T-2014. In addition to coastal waters, the highest latitudes of the Arctic and the Mediterranean Sea are also excluded as in all previous LDEO climatologies.

To develop a climatology from data collected over multiple decades during which $f\text{CO}_2$ experienced a large secular trend, we calculate $\Delta f\text{CO}_2$ values for each day and grid cell before collapsing all available data onto one climatological year. This method follows the assumption made in previous iterations of this climatology (T-1997) that the ocean surface carbon value follows the rate of increase in the atmospheric

$f\text{CO}_2$, such that $\Delta f\text{CO}_2$ is constant over time. Observed $\Delta f\text{CO}_2$ is then interpolated in space–time using a lateral two-dimensional diffusion–advection equation on a $4^\circ \times 5^\circ$ grid (Takahashi et al., 1995; T-1997; T-2002; T-2009a; T-2014). Monthly mean $\Delta f\text{CO}_2$ values for each pixel, down-scaled to $1^\circ \times 1^\circ$ resolution, are presented here. Net sea–air CO_2 flux is computed using the pySeaFlux package, following the protocol presented in Fay et al. (2021).

Regional mean $\Delta f\text{CO}_2$ values vary greatly among the ocean basins (Figs. 3 and 4). The high-latitude North Atlantic is the most intense CO_2 sink per unit area as a result of both highly negative $\Delta f\text{CO}_2$ (Fig. 3) and strong winds. This is also the region with the largest differences between the climatologies created with previous versions of the LDEO database and this version based on the SOCATv2022 database (Figs. 3 and 7). Globally, differences are due to the greater abundance of observations over all regions of the global oceans in the SOCAT database, but particularly the greater seasonal coverage in the Southern Hemisphere oceans and subpolar North Atlantic (Figs. 1, S1).

The annual mean uptake flux for the global open ocean region is estimated to be $-1.79 \pm 0.7 \text{Pg C yr}^{-1}$ for 1980–2021 (Figs. 5 and 6). Of the major ocean basins, the Southern Hemisphere ocean (south of 30°S) is the largest CO_2 sink, taking up 1.22Pg C yr^{-1} , while the Northern Hemisphere ocean (north of 30°N) takes up 0.93Pg C yr^{-1} . The equatorial ocean region acts as the only year-round region of carbon efflux to the atmosphere and emits 0.36Pg C to the atmosphere annually.

While over a million new shipboard $f\text{CO}_2^{\text{oc}}$ observations have been made each year in the global oceans for the past 2 decades, there has been a notable decline in the observations submitted to SOCAT since 2017 (Bakker et al., 2022, 2023). This decline is due in part to the disruption by the COVID-19 pandemic but also reflects a shift away from shipboard $p\text{CO}_2$ measurements. Given the lack of alternative approaches with which to assess spatial and temporal variability in air–sea CO_2 flux and the need for high accuracy shipboard measurements (accuracy of $< 2 \mu\text{atm}$) to characterize most regions of the global oceans, this trend to fewer observations is highly detrimental to carbon cycle research. This is true both in regard to monitoring of ocean carbon uptake and to monitoring of more uncertain fluxes such as those between the atmosphere and terrestrial biosphere since the high uncertainty of independent terrestrial estimates necessitates the monitoring of this flux by difference.

Supplement. The supplement related to this article is available online at: <https://doi.org/10.5194/essd-16-2123-2024-supplement>.

Author contributions. ARF and DRM conducted the analysis and prepared the manuscript. GAM, RW, CS, SCS, and DP con-

tributed ideas and provided feedback throughout the analysis as well as contributed to the manuscript.

Disclaimer. Publisher’s note: Copernicus Publications remains neutral with regard to jurisdictional claims made in the text, published maps, institutional affiliations, or any other geographical representation in this paper. While Copernicus Publications makes every effort to include appropriate place names, the final responsibility lies with the authors.

Acknowledgements. The Surface Ocean CO_2 Atlas (SOCAT) is an international effort, endorsed by the International Ocean Carbon Coordination Project (IOCCP), the Surface Ocean Lower Atmosphere Study (SOLAS), and the Integrated Marine Biosphere Research (IMBeR) program, to deliver a uniformly quality-controlled surface ocean CO_2 database. The many researchers and funding agencies responsible for the collection of data and quality control are thanked for their contributions to SOCAT.

Financial support. This research has been supported by the Global Ocean Monitoring and Observing Program (grant no. 100007298).

Review statement. This paper was edited by François G. Schmitt and reviewed by two anonymous referees.

References

- Atlas, R., Hoffman, R. N., Ardizzone, J., Leidner, S. M., Jusem, J. C., Smith, D. K., and Gombos, D.: A cross-calibrated, multi-platform ocean surface wind velocity product for meteorological and oceanographic applications, *B. Am. Meteorol. Soc.*, 92, 157–174, <https://doi.org/10.1175/2010BAMS2946.1>, 2011.
- Ayers, J. M. and Lozier, M. S.: Unraveling dynamical controls on the North Pacific carbon sink, *J. Geophys. Res.-Oceans*, 117, <https://doi.org/10.1029/2011JC007368>, 2012.
- Bakker, D. C. E., Pfeil, B., Landa, C. S., Metzl, N., O’Brien, K. M., Olsen, A., Smith, K., Cosca, C., Harasawa, S., Jones, S. D., Nakaoka, S., Nojiri, Y., Schuster, U., Steinhoff, T., Sweeney, C., Takahashi, T., Tilbrook, B., Wada, C., Wanninkhof, R., Alin, S. R., Balestrini, C. F., Barbero, L., Bates, N. R., Bianchi, A. A., Bonou, F., Boutin, J., Bozec, Y., Burger, E. F., Cai, W.-J., Castle, R. D., Chen, L., Chierici, M., Currie, K., Evans, W., Featherstone, C., Feely, R. A., Fransson, A., Goyet, C., Greenwood, N., Gregor, L., Hankin, S., Hardman-Mountford, N. J., Harlay, J., Hauck, J., Hoppema, M., Humphreys, M. P., Hunt, C. W., Huss, B., Ibáñez, J. S. P., Johannessen, T., Keeling, R., Kitidis, V., Körtzinger, A., Kozyr, A., Krasakopoulou, E., Kuwata, A., Landschützer, P., Lauvset, S. K., Lefèvre, N., Lo Monaco, C., Manke, A., Mathis, J. T., Merlivat, L., Millero, F. J., Monteiro, P. M. S., Munro, D. R., Murata, A., Newberger, T., Omar, A. M., Ono, T., Paterson, K., Pearce, D., Pierrot, D., Robbins, L. L., Saito, S., Salisbury, J., Schlitzer, R., Schneider, B., Schweitzer, R., Sieger, R., Skjelvan, I., Sullivan, K. F., Sutherland, S. C., Sutton, A. J., Tadokoro, K., Telszewski, M., Tuma, M., van Heuven, S. M. A. C., Vandemark, D., Ward, B., Watson, A. J., and Xu, S.: A multi-decade record of high-quality $f\text{CO}_2$ data in version 3 of the Surface Ocean CO_2 Atlas (SOCAT), *Earth Syst. Sci. Data*, 8, 383–413, <https://doi.org/10.5194/essd-8-383-2016>, 2016.
- Bakker, D. C. E., Alin, S. R., Becker, M., Bittig, H. C., Castaño-Primo, R., Feely, R. A., Gkritzalis, T., Kadono, K., Kozyr, A., Lauvset, S. K., Metzl, N., Munro, D. R., Nakaoka, S., Nojiri, Y., O’Brien, K. M., Olsen, A., Pfeil, B., Pierrot, D., Steinhoff, T., Sullivan, K. F., Sutton, A. J., Sweeney, C., Tilbrook, B., Wada, C., Wanninkhof, R., Willstrand Wranne, A., Akl, J., Apelthun, L. B., Bates, N., Beatty, C. M., Burger, E. F., Cai, W., Cosca, C. E., Corredor, J. E., Cronin, M., Cross, J. N., De Carlo, E. H., DeGrandpre, M. D., Emerson, S. R., Enright, M. P., Enyo, K., Evans, W., Frangoulis, C., Fransson, A., García-Ibáñez, M. I., Gehrung, M., Giannoudi, L., Glockzin, M., Hales, B., Howden, S. D., Hunt, C. W., Ibáñez, J. S. P., Jones, S. D., Kamb, L., Körtzinger, A., Landa, C. S., Landschützer, P., Lefèvre, N., Lo Monaco, C., Macovei, V. A., Maenner, A., Jones, S., Meinig, C., Millero, F. J., Monacci, N. M., Mordy, C., Morell, J. M., Murata, A., Musielewicz, S., Neill, C., Newberger, T., Nomura, D., Ohman, M., Ono, T., Passmore, A., Petersen, W., Petihakis, G., Perivoliotis, L., Plueddemann, A. J., Rehder, G., Reynaud, T., Rodriguez, C., Ross, A. C., Rutgersson, A., Sabine, C. L., Salisbury, J. E., Schlitzer, R., Send, U., Skjelvan, I., Stamatakis, N., Sutherland, S. C., Tadokoro, K., Tanhua, T., Telszewski, M., Trull, T., Vandemark, D., van Ooijen, E., Voynova, Y. G., Wang, H., Weller, R. A., Whitehead, C. S., and Wilson, D.: Surface Ocean CO_2 Atlas Database Version 2022 (SOCATv2022) (NCEI Accession 0253659), NOAA National Centers for Environmental Information [data set], <https://doi.org/10.25921/1h9f-nb73>, 2022.
- Bakker, D., Sanders, R., Collins, A., DeGrandpre, M., Gkritzalis, T., Ibáñez, S., Jones, S., Lauvset, S., Metzl, N., O’Brien, K., Olsen, A., Schuster, U., Steinhoff, T., Telszewski, M., Tilbrook, B., and Wallace, D.: Case for SOCAT as an integral part of the value chain advising UNFCCC on ocean CO_2 uptake, http://www.ioccp.org/images/Gnews/2023_A_Case_for_SOCAT.pdf (last access: 18 September 2023), 2023.
- Bates, N. R., Astor, Y. M., Church, M. J., Currie, K., Dore, J. E., Gonzalez-Davila, M., Lorenzoni, L., Muller-Karger, F., Olafsson, J., and Santana-Casiano, J. M.: A Time-Series View of Changing Surface Ocean Chemistry Due to Ocean Uptake of Anthropogenic CO_2 and Ocean Acidification, *Oceanography*, 27, 126–141, 2014.
- Chen, C. T. A. and Tsunogai, S.: Carbon and nutrients in the ocean, in: *Asian Change in the Context of Global Change*, edited by: Galloway, J. N. and Melillo, J. M., 271–307, Cambridge University Press., 2019.
- DeVries, T., Yamamoto, K., Wanninkhof, R., Gruber, N., Hauck, J., Müller, J. D., Bopp, L., Carroll, D., Carter, B., Chau, T., Doney, S., Gehlen, M., Gloege, L., Gregor, L., Henson, S., Kim, J. H., Iida, Y., Ilyina, T., Landschützer, P., Le Quéré, C., Munro, D., Nissen, C., Patara, L., Perez, F. F., Resplandy, L., Rodgers, K., Schwinger, J., Séférian, R., Sicardi, V., Terhaar, J., Triñanes, J., Tsujino, H., Watson, A., Yasunaka, S., and Zeng, J.: Magnitude, trends, and variability of the global ocean carbon sink from

- 1985–2018, *Global Biogeochem. Cycles*, 37, e2023GB007780, <https://doi.org/10.1029/2023GB007780>, 2023.
- Dickson, A. G., Sabine, C. L., and Christian, J. R. (Eds.): Guide to best practices for ocean CO_2 measurements, PICES Special Publication 3, IOCCP Report 8, 191 pp., 2007.
- Fay, A. R. and McKinley, G. A.: Global trends in surface ocean $p\text{CO}_2$ from in situ data, *Global Biogeochem. Cycles*, 27, 541–557, 2013.
- Fay, A. R. and McKinley, G. A.: Global open-ocean biomes: mean and temporal variability, *Earth Syst. Sci. Data*, 6, 273–284, <https://doi.org/10.5194/essd-6-273-2014>, 2014.
- Fay, A. R., Gregor, L., Landschützer, P., McKinley, G. A., Gruber, N., Gehlen, M., Iida, Y., Laruelle, G. G., Rödenbeck, C., Roobaert, A., and Zeng, J.: SeaFlux: harmonization of air–sea CO_2 fluxes from surface $p\text{CO}_2$ data products using a standardized approach, *Earth Syst. Sci. Data*, 13, 4693–4710, <https://doi.org/10.5194/essd-13-4693-2021>, 2021.
- Fay, A. R., Munro, D. R., McKinley, G. A., Pierrot, D., Sutherland, S. C., Sweeney, C., and Wanninkhof, R.: Climatological distributions of sea–air $\Delta f\text{CO}_2$ and CO_2 flux densities in the Global Surface Ocean (NCEI Accession 0282251), NOAA National Centers for Environmental Information [data set], <https://doi.org/10.25921/295g-sn13>, 2023.
- Feng, S., Lauvaux, T., Keller, K., Davis, K. J., Rayner, P., Oda, T., and Gurney, K. R.: A road map for improving the treatment of uncertainties in high-resolution regional carbon flux inverse estimates, *Geophys. Res. Lett.*, 46, 13461–13469, <https://doi.org/10.1029/2019GL082987>, 2019.
- Friedlingstein, P., O’Sullivan, M., Jones, M. W., Andrew, R. M., Gregor, L., Hauck, J., Le Quéré, C., Luijkx, I. T., Olsen, A., Peters, G. P., Peters, W., Pongratz, J., Schwingshackl, C., Sitch, S., Canadell, J. G., Ciais, P., Jackson, R. B., Alin, S. R., Alkama, R., Arneeth, A., Arora, V. K., Bates, N. R., Becker, M., Bellouin, N., Bittig, H. C., Bopp, L., Chevallier, F., Chini, L. P., Cronin, M., Evans, W., Falk, S., Feely, R. A., Gasser, T., Gehlen, M., Gkritzalis, T., Gloege, L., Grassi, G., Gruber, N., Gürses, Ö., Harris, I., Hefner, M., Houghton, R. A., Hurtt, G. C., Iida, Y., Ilyina, T., Jain, A. K., Jersild, A., Kadono, K., Kato, E., Kennedy, D., Klein Goldewijk, K., Knauer, J., Korsbakken, J. I., Landschützer, P., Lefèvre, N., Lindsay, K., Liu, J., Liu, Z., Marland, G., Mayot, N., McGrath, M. J., Metzl, N., Monacchi, N. M., Munro, D. R., Nakaoka, S.-I., Niwa, Y., O’Brien, K., Ono, T., Palmer, P. I., Pan, N., Pierrot, D., Pockock, K., Poulter, B., Resplandy, L., Robertson, E., Rödenbeck, C., Rodriguez, C., Rosan, T. M., Schwinger, J., Séférian, R., Shutler, J. D., Skjelvan, I., Steinhoff, T., Sun, Q., Sutton, A. J., Sweeney, C., Takao, S., Tanhua, T., Tans, P. P., Tian, X., Tian, H., Tilbrook, B., Tsujino, H., Tubiello, F., van der Werf, G. R., Walker, A. P., Wanninkhof, R., Whitehead, C., Willstrand Wranne, A., Wright, R., Yuan, W., Yue, C., Yue, X., Zaehle, S., Zeng, J., and Zheng, B.: Global Carbon Budget 2022, *Earth Syst. Sci. Data*, 14, 4811–4900, <https://doi.org/10.5194/essd-14-4811-2022>, 2022.
- Gloege, L., McKinley, G. A., Landschützer, P., Fay, A. R., Frolicher, T., Fyfe, J., Ilyina, T., Jones, S., Lovenduski, N. S., Rödenbeck, C., Rogers, K., Schlunegger, S., and Takano, Y.: Quantifying errors in observationally-based estimates of ocean carbon sink variability, *Global Biogeochem. Cy.*, 35, e2020GB006788, <https://doi.org/10.1029/2020GB006788>, 2021.
- Good, S. A., Martin, M. J., and Rayner, N. A.: EN4: Quality controlled ocean temperature and salinity profiles and monthly objective analyses with uncertainty estimates, *J. Geophys. Res.-Oceans*, 118, 6704–6716, <https://doi.org/10.1002/2013JC009067>, 2013.
- Gregor, L. and Fay, A. R.: SeaFlux data set: harmonised sea–air CO_2 fluxes from surface $p\text{CO}_2$ data products using a standardised approach (2021.04), Zenodo [data set], <https://doi.org/10.5281/zenodo.5148460>, 2021.
- Gruber, N., Clement, D., Carter, B. R., Feely, R. A., Van Heuven, S., Hoppema, M., Ishii, M., Key, R. M., Kozyr, A., Lauvset, S. K., and Lo Monaco, C.: The oceanic sink for anthropogenic CO_2 from 1994 to 2007, *Science*, 363, 1193–1199, <https://doi.org/10.1126/science.aau5153>, 2019.
- Gruber, N., Bakker, D. C., DeVries, T., Gregor, L., Hauck, J., Landschützer, P., McKinley, G. A., and Müller, J. D.: Trends and variability in the ocean carbon sink, *Nat. Rev. Earth Environ.*, 4, 119–134, <https://doi.org/10.1038/s43017-022-00381-x>, 2023.
- Hauck, J., Zeising, M., Le Quéré, C., Gruber, N., Bakker, D. C. E., Bopp, L., Chau, T. T. T., Gürses, Ö., Ilyina, T., Landschützer, P., Lenton, A., Resplandy, L., Rödenbeck, C., Schwinger, J., and Séférian, R.: Consistency and Challenges in the Ocean Carbon Sink Estimate for the Global Carbon Budget, *Front. Mar. Sci.*, 7, 852–885, <https://doi.org/10.3389/fmars.2020.571720>, 2020.
- Hersbach, H., Bell, B., Berrisford, P., Biavati, G., Horányi, A., Muñoz Sabater, J., Nicolas, J., Peubey, C., Radu, R., Rozum, I., Schepers, D., Simmons, A., Soci, C., Dee, D., and Thépaut, J.-N.: ERA5 monthly averaged data on single levels from 1940 to present, Copernicus Climate Change Service (C3S) Climate Data Store (CDS) [data set], <https://doi.org/10.24381/cds.f17050d7> (last access: 16 October 2020), 2023.
- Ho, D. T., Wanninkhof, R., Schlosser, P., Ullman, D. S., Hebert, D., and Sullivan, K. F.: Towards a universal relationship between wind speed and gas exchange: Gas transfer velocities measured with $^3\text{He}/\text{SF}_6$ during the Southern Ocean Gas Exchange Experiment, *J. Geophys. Res.*, 116, C00F04, <https://doi.org/10.1029/2010JC006854>, 2011.
- Jacobson, A. R., Mikaloff-Fletcher, S. E., Gruber, N., Sarmiento, J. S., and Gloor, M.: A joint atmosphere–ocean inversion for surface fluxes of carbon dioxide: 1. Methods and global-scale fluxes, *Global Biogeochem. Cy.*, 21, GB1019, <https://doi.org/10.1029/2005GB002556>, 2007.
- Kobayashi, S., Ota, Y., Harada, Y., Ebata, A., Moriwa, M., Onoda, H., Onogi, K., Kamahori, H., Kobayashi, C., Endo, H., Miyaoka, K., and Takahashi, K.: The JRA-55 Reanalysis: General Specifications and Basic Characteristics, *J. Meteorol. Soc. Jpn.*, 93, 5–48, <https://doi.org/10.2151/jmsj.2015-001>, 2015.
- Lan, X., Tans, P., Thoning, K., and NOAA Global Monitoring Laboratory: NOAA Greenhouse Gas Marine Boundary Layer Reference – CO_2 , NOAA GML [data set], <https://doi.org/10.15138/DVNP-F961>, 2023.
- Landschützer, P., Gruber, N., and Bakker, D. C.: Decadal variations and trends of the global ocean carbon sink, *Global Biogeochem. Cycles*, 30, 1396–1417, 2016.
- Landschützer, P., Laruelle, G. G., Roobaert, A., and Regnier, P.: A uniform $p\text{CO}_2$ climatology combining open and coastal oceans, *Earth Syst. Sci. Data*, 12, 2537–2553, <https://doi.org/10.5194/essd-12-2537-2020>, 2020.

- Manning, A. C. and Keeling, R. F.: Global oceanic and land biotic carbon sinks from the Scripps atmospheric oxygen flask sampling network, *Tellus*, 58B, 95–116, 2006.
- McKinley, G. A., Fay, A. R., Eddebbbar, Y. A., Gloege, L., and Lovenduski, N. S.: External forcing explains recent decadal variability of the ocean carbon sink, *AGU Adv.*, 1, e2019AV000149, <https://doi.org/10.1029/2019AV000149>, 2020.
- Pfeil, B., Olsen, A., Bakker, D. C. E., Hankin, S., Koyuk, H., Kozyr, A., Malczyk, J., Manke, A., Metzl, N., Sabine, C. L., Akl, J., Alin, S. R., Bates, N., Bellerby, R. G. J., Borges, A., Boutin, J., Brown, P. J., Cai, W.-J., Chavez, F. P., Chen, A., Cosca, C., Fassbender, A. J., Feely, R. A., González-Dávila, M., Goyet, C., Hales, B., Hardman-Mountford, N., Heinze, C., Hood, M., Hoppema, M., Hunt, C. W., Hydes, D., Ishii, M., Johannessen, T., Jones, S. D., Key, R. M., Körtzinger, A., Landschützer, P., Lauvset, S. K., Lefèvre, N., Lenton, A., Lourantou, A., Merlivat, L., Midorikawa, T., Mintrop, L., Miyazaki, C., Murata, A., Nakadate, A., Nakano, Y., Nakaoka, S., Nojiri, Y., Omar, A. M., Padin, X. A., Park, G.-H., Paterson, K., Perez, F. F., Pierrot, D., Poisson, A., Ríos, A. F., Santana-Casiano, J. M., Salisbury, J., Sarma, V. V. S. S., Schlitzer, R., Schneider, B., Schuster, U., Sieger, R., Skjelvan, I., Steinhoff, T., Suzuki, T., Takahashi, T., Tedesco, K., Telszewski, M., Thomas, H., Tilbrook, B., Tjiputra, J., Vandemark, D., Veness, T., Wanninkhof, R., Watson, A. J., Weiss, R., Wong, C. S., and Yoshikawa-Inoue, H.: A uniform, quality controlled Surface Ocean CO_2 Atlas (SOCAT), *Earth Syst. Sci. Data*, 5, 125–143, <https://doi.org/10.5194/essd-5-125-2013>, 2013.
- Quay, P. D., Tilbrook, B., and Wong C. S.: Oceanic uptake of fossil fuel CO_2 : carbon-13 evidence, *Science*, 256, 74–79, 1992.
- Reynolds, R. W., Rayner, N. A., Smith, T. M., Stokes, D. C., and Wang, W.: An improved in situ and satellite SST analysis for climate, *J. Climate*, 15, 1609–1625, [https://doi.org/10.1175/1520-0442\(2002\)015<1609:AISAS>2.0.CO;2](https://doi.org/10.1175/1520-0442(2002)015<1609:AISAS>2.0.CO;2), 2002 (data available at: <https://psl.noaa.gov/data/gridded/data.noaa.oisst.v2.html>, last access: 26 April 2021).
- Ridge, S. M. and McKinley, G. A.: Advective Controls on the North Atlantic Anthropogenic Carbon Sink. *Global Biogeochem. Cycles*, 34, 1138, <https://doi.org/10.1029/2019gb006457>, 2020.
- Rödenbeck, C., Bakker, D. C. E., Gruber, N., Iida, Y., Jacobson, A. R., Jones, S., Landschützer, P., Metzl, N., Nakaoka, S., Olsen, A., Park, G.-H., Peylin, P., Rodgers, K. B., Sasse, T. P., Schuster, U., Shutler, J. D., Valsala, V., Wanninkhof, R., and Zeng, J.: Data-based estimates of the ocean carbon sink variability – first results of the Surface Ocean $p\text{CO}_2$ Mapping intercomparison (SOCOM), *Biogeosciences*, 12, 7251–7278, <https://doi.org/10.5194/bg-12-7251-2015>, 2015.
- Sabine, C. L., Wanninkhof, R., Key, R. M., Goyet, C., and Millero, F. J.: Seasonal CO_2 fluxes in the tropical and subtropical Indian Ocean, *Marine Chem.*, 72, 33–53, [https://doi.org/10.1016/s0304-4203\(00\)00064-5](https://doi.org/10.1016/s0304-4203(00)00064-5), 2000.
- Sabine, C. L., Hankin, S., Koyuk, H., Bakker, D. C. E., Pfeil, B., Olsen, A., Metzl, N., Kozyr, A., Fassbender, A., Manke, A., Malczyk, J., Akl, J., Alin, S. R., Bellerby, R. G. J., Borges, A., Boutin, J., Brown, P. J., Cai, W.-J., Chavez, F. P., Chen, A., Cosca, C., Feely, R. A., González-Dávila, M., Goyet, C., Hardman-Mountford, N., Heinze, C., Hoppema, M., Hunt, C. W., Hydes, D., Ishii, M., Johannessen, T., Key, R. M., Körtzinger, A., Landschützer, P., Lauvset, S. K., Lefèvre, N., Lenton, A., Lourantou, A., Merlivat, L., Midorikawa, T., Mintrop, L., Miyazaki, C., Murata, A., Nakadate, A., Nakano, Y., Nakaoka, S., Nojiri, Y., Omar, A. M., Padin, X. A., Park, G.-H., Paterson, K., Perez, F. F., Pierrot, D., Poisson, A., Ríos, A. F., Santana-Casiano, J. M., Salisbury, J., Sarma, V. V. S. S., Schlitzer, R., Schneider, B., Schuster, U., Sieger, R., Skjelvan, I., Steinhoff, T., Suzuki, T., Takahashi, T., Tedesco, K., Telszewski, M., Thomas, H., Tilbrook, B., Tjiputra, J., Vandemark, D., Veness, T., Wanninkhof, R., Watson, A. J., Weiss, R., Wong, C. S., and Yoshikawa-Inoue, H.: A uniform, quality controlled Surface Ocean CO_2 Atlas (SOCAT), *Earth Syst. Sci. Data*, 5, 125–143, <https://doi.org/10.5194/essd-5-125-2013>, 2013.
- Quay, P. D., Tilbrook, B., and Wong C. S.: Oceanic uptake of fossil fuel CO_2 : carbon-13 evidence, *Science*, 256, 74–79, 1992.
- Reynolds, R. W., Rayner, N. A., Smith, T. M., Stokes, D. C., and Wang, W.: An improved in situ and satellite SST analysis for climate, *J. Climate*, 15, 1609–1625, [https://doi.org/10.1175/1520-0442\(2002\)015<1609:AISAS>2.0.CO;2](https://doi.org/10.1175/1520-0442(2002)015<1609:AISAS>2.0.CO;2), 2002 (data available at: <https://psl.noaa.gov/data/gridded/data.noaa.oisst.v2.html>, last access: 26 April 2021).
- Ridge, S. M. and McKinley, G. A.: Advective Controls on the North Atlantic Anthropogenic Carbon Sink. *Global Biogeochem. Cycles*, 34, 1138, <https://doi.org/10.1029/2019gb006457>, 2020.
- Rödenbeck, C., Bakker, D. C. E., Gruber, N., Iida, Y., Jacobson, A. R., Jones, S., Landschützer, P., Metzl, N., Nakaoka, S., Olsen, A., Park, G.-H., Peylin, P., Rodgers, K. B., Sasse, T. P., Schuster, U., Shutler, J. D., Valsala, V., Wanninkhof, R., and Zeng, J.: Data-based estimates of the ocean carbon sink variability – first results of the Surface Ocean $p\text{CO}_2$ Mapping intercomparison (SOCOM), *Biogeosciences*, 12, 7251–7278, <https://doi.org/10.5194/bg-12-7251-2015>, 2015.
- Sabine, C. L., Wanninkhof, R., Key, R. M., Goyet, C., and Millero, F. J.: Seasonal CO_2 fluxes in the tropical and subtropical Indian Ocean, *Marine Chem.*, 72, 33–53, [https://doi.org/10.1016/s0304-4203\(00\)00064-5](https://doi.org/10.1016/s0304-4203(00)00064-5), 2000.
- Sabine, C. L., Hankin, S., Koyuk, H., Bakker, D. C. E., Pfeil, B., Olsen, A., Metzl, N., Kozyr, A., Fassbender, A., Manke, A., Malczyk, J., Akl, J., Alin, S. R., Bellerby, R. G. J., Borges, A., Boutin, J., Brown, P. J., Cai, W.-J., Chavez, F. P., Chen, A., Cosca, C., Feely, R. A., González-Dávila, M., Goyet, C., Hardman-Mountford, N., Heinze, C., Hoppema, M., Hunt, C. W., Hydes, D., Ishii, M., Johannessen, T., Key, R. M., Körtzinger, A., Landschützer, P., Lauvset, S. K., Lefèvre, N., Lenton, A., Lourantou, A., Merlivat, L., Midorikawa, T., Mintrop, L., Miyazaki, C., Murata, A., Nakadate, A., Nakano, Y., Nakaoka, S., Nojiri, Y., Omar, A. M., Padin, X. A., Park, G.-H., Paterson, K., Perez, F. F., Pierrot, D., Poisson, A., Ríos, A. F., Santana-Casiano, J. M., Salisbury, J., Sarma, V. V. S. S., Schlitzer, R., Schneider, B., Schuster, U., Sieger, R., Skjelvan, I., Steinhoff, T., Suzuki, T., Takahashi, T., Tedesco, K., Telszewski, M., Thomas, H., Tilbrook, B., Tjiputra, J., Vandemark, D., Veness, T., Wanninkhof, R., Watson, A. J., Weiss, R., Wong, C. S., and Yoshikawa-Inoue, H.: Surface Ocean CO_2 Atlas (SOCAT) gridded data products, *Earth Syst. Sci. Data*, 5, 145–153, <https://doi.org/10.5194/essd-5-145-2013>, 2013.
- Takahashi, T., Olafsson, J., Goddard, J. G., Chipman, D. W., and Sutherland, S. C.: Seasonal variation of CO_2 and nutrients in the high-latitude surface oceans: A comparative study, *Global Biogeochem. Cycles*, 7, 843–878, 1993.
- Takahashi, T., Takahashi, T. T., and Sutherland, S. C.: An assessment of the role of the North Atlantic as a CO_2 sink, *Philos. T. Roy. Soc. Lond. B*, 348, 143–152, 1995.
- Takahashi, T., Feely, R. A., Weiss, R. F., Wanninkhof, R. H., Chipman, D. W., Sutherland, S. C., and Takahashi, T. T.: Global air-sea flux of CO_2 : An estimate based on measurements of sea–air $p\text{CO}_2$ difference, *P. Natl. Acad. Sci. USA*, 94, 8292–8299, 1997.
- Takahashi, T., Sutherland, S. C., Sweeney, C., Poisson, A., Metzl, N., Tilbrook, B., Bates, N., Wanninkhof, R., Feely, R. A., Sabine, C., and Olafsson, J.: Global sea–air CO_2 flux based on climatological surface ocean $p\text{CO}_2$, and seasonal biological and temperature effects, *Deep-Sea Res. Pt. II*, 49, 1601–1622, 2002.
- Takahashi, T., Sutherland, S. C., Wanninkhof, R., Sweeney, C., Feely, R. A., Chipman, D. W., Hales, B., Friederich, G., Chavez, F., Sabine, C., Watson, A., Bakker, D. C. E., Schuster, U., Metzl, N., Yoshikawa-Inoue, H., Ishii, M., Midorikawa, T., Nojiri, Y., Körtzinger, A., Steinhoff, T., Hoppema, M., Olafsson, J., Arnarson, T. S., Tilbrook, B., Johannessen, T., Olsen, A., Bellerby, R., Wong, C. S., Delille, B., Bates, N. R., and de Baar, H. J. W.: Climatological mean and decadal change in surface ocean $p\text{CO}_2$, and net sea–air CO_2 flux over the global oceans, *Deep-Sea Res. Pt. II*, 56, 554–577, <https://doi.org/10.1016/j.dsr2.2008.12.009>, 2009a.
- Takahashi, T., Sutherland, S. C., Wanninkhof, R., Sweeney, C., Feely, R. A., Chipman, D. W., Hales, B., Friederich, G., Chavez, F., Sabine, C., Watson, A., Bakker, D. C. E., Schuster, U., Metzl, N., Yoshikawa-Inoue, H., Ishii, M., Midorikawa, T., Nojiri, Y., Körtzinger, A., Steinhoff, T., Hoppema, M., Olafsson, J., Arnarson, T. S., Tilbrook, B., Johannessen, T., Olsen, A., Bellerby, R., Wong, C. S., Delille, B., Bates, N. R., and de Baar, H. J. W.: Corrigendum to “Climatological mean and decadal change in surface ocean $p\text{CO}_2$, and net sea–air CO_2 flux over the global oceans”, *Deep-Sea Res. Pt. I*, 56, 2075–2076, <https://doi.org/10.1016/j.dsr.2009.07.007>, 2009b.
- Takahashi, T., Sutherland, S. C., Chipman, D. W., Goddard, J. G., Ho, C., Newberger, T., Sweeney, C., and Munro, D. R.: Climatological distributions of pH, $p\text{CO}_2$, total CO_2 , alkalinity, and CaCO_3 saturation in the global surface ocean, and temporal changes at selected locations, *Marine Chem.*, 164, 95–125, <https://doi.org/10.1016/j.marchem.2014.06.004>, 2014.
- Takahashi, T., Sutherland, S. C., and Kozyr, A.: Global Ocean Surface Water Partial Pressure of CO_2 Database: Measurements Performed During 1957–2019 (LDEO Database Version 2019) (NCEI Accession 0160492), Version 9.9, NOAA

- National Centers for Environmental Information [data set], [https://doi.org/10.3334/CDIAC/OTG.NDP088\(V2015\)](https://doi.org/10.3334/CDIAC/OTG.NDP088(V2015)), 2021.
- Tanhua, T., Orr, J. C., Lorenzoni, L., and Hansson, L.: Monitoring ocean carbon and ocean acidification, *WMO Bulletin*, 64, 48–51, https://library.wmo.int/viewer/58572/download?file=bulletin_64-1_en.pdf&type=pdf&navigator=1 (last access: 18 September 2023), 2015.
- Tans, P. P., Fung, I. Y., and Takahashi, T.: Observational Constrains on the Global Atmospheric CO_2 Budget, *Science*, 247, 1431–1438, <https://doi.org/10.1126/science.247.4949.1431>, 1990.
- Tans, P. P., Berry, J. A., and Keeling, R. F.: Oceanic $^{13}\text{C}/^{12}\text{C}$ observations: a new window on ocean CO_2 uptake, *Global Biogeochem. Cycles*, 7, 353–368, 1993.
- Tjiputra, J. F., Olsen, A., Bopp, L., Lenton, A., Pfeil, B., Roy, T., Segsneider, J., Totterdell, I., and Heinze, C.: Long-term surface pCO_2 trends from observations and models, *Tellus B*, 66, 23083, <https://doi.org/10.3402/tellusb.v66.23083>, 2014.
- Wanninkhof, R.: Relationship between wind speed and gas exchange over the ocean revisited, *Limnol. Oceanogr. Methods*, 12, 351–362, <https://doi.org/10.4319/lom.2014.12.351>, 2014.
- Wanninkhof, R., Park, G.-H., Takahashi, T., Sweeney, C., Feely, R., Nojiri, Y., Gruber, N., Doney, S. C., McKinley, G. A., Lenton, A., Le Quéré, C., Heinze, C., Schwinger, J., Graven, H., and Khatiwala, S.: Global ocean carbon uptake: magnitude, variability and trends, *Biogeosciences*, 10, 1983–2000, <https://doi.org/10.5194/bg-10-1983-2013>, 2013.
- Weiss, R.: Carbon dioxide in water and seawater: the solubility of non-ideal gas, *Mar. Chem.*, 2, 203–215, [https://doi.org/10.1016/0304-4203\(74\)90015-2](https://doi.org/10.1016/0304-4203(74)90015-2), 1974.